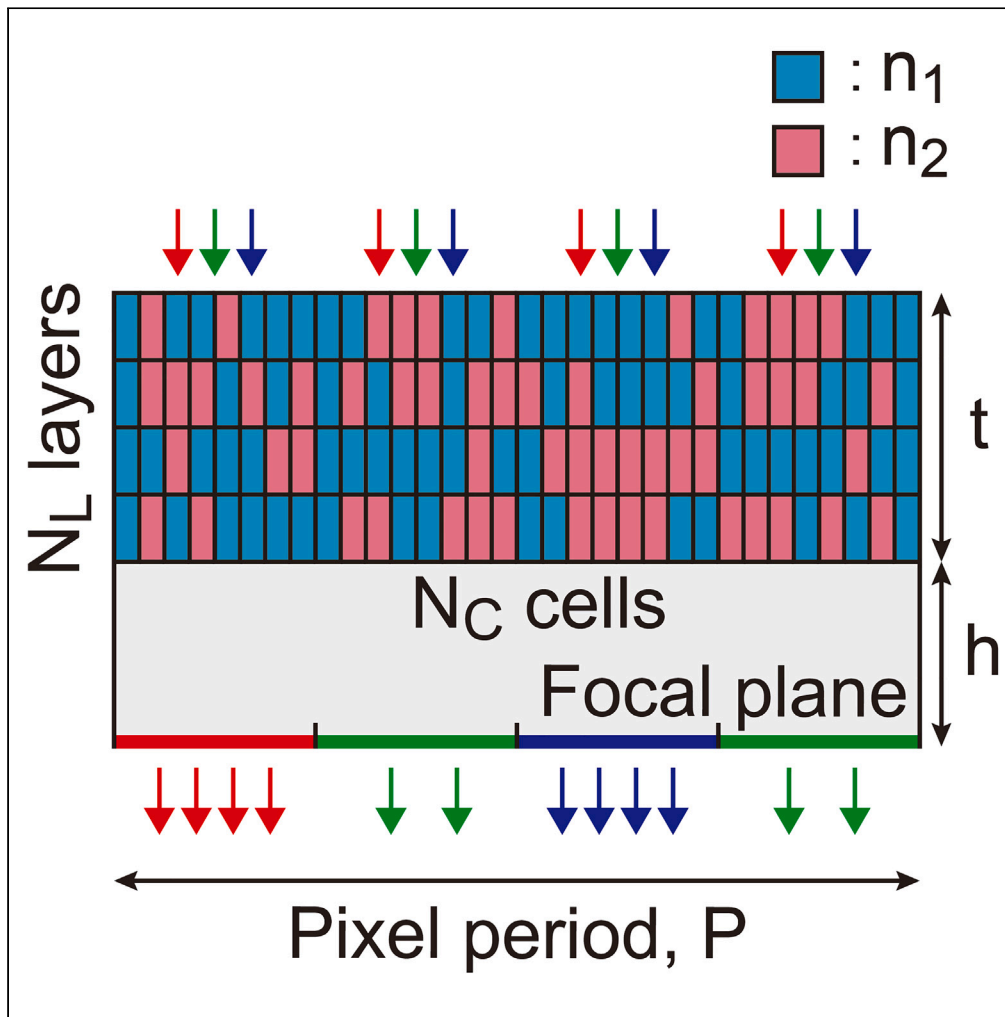


Article

Design parameters of free-form color splitters for subwavelength pixelated image sensors



Sanmun Kim,
Chanyung Park,
Shinho Kim,
Haejun Chung,
Min Seok Jang

jang.minseok@kaist.ac.kr

Highlights

The optimization of metasurface-based color splitters is conducted

The influence of design parameters on optimized optical efficiency is examined

There exist optimal ranges of structural parameters and the optical index contrast

The number of layers plays a crucial role in determining device performance



Article

Design parameters of free-form color splitters for subwavelength pixelated image sensors

Sanmun Kim,^{1,4} Chanhyung Park,^{1,4} Shinho Kim,¹ Haejun Chung,^{2,3} and Min Seok Jang^{1,5,*}

SUMMARY

Metasurface-based color splitters are emerging as next-generation optical components for image sensors, replacing classical color filters and microlens arrays. In this work, we report how the design parameters such as the device dimensions and refractive indices of the dielectrics affect the optical efficiency of the color splitters. Also, we report how the design grid resolution parameters affect the optical efficiency and discover that the fabrication of a color splitter is possible even in legacy fabrication facilities with low structure resolutions.

INTRODUCTION

The major optical components in classical image sensors are a microlens array and color filter. A microlens focuses the incident light on the photodiode and the color filter blocks the light of unwanted wavelength (Figure 1A). However, such geometric optics-based configuration is limited to image sensors with pixel sizes relatively large compared to the wavelength.^{1,2} Recent developments in image sensors brought the subpixel size down to 0.56 μm ,³ reaching down to the boundary of the geometric optics and wave optics. Further miniaturization will likely cause a failure in design approaches based on geometric optics. Furthermore, a decrease in the subpixel size has led to a reduction of light energy per subpixel leading to poor image quality. Metasurface-based color splitters are being investigated as a candidate for substituting microlenses and color filters due to their high optical efficiency. Instead of filtering out lights of unwanted wavelength, the color splitter guides the incoming light to the corresponding subpixels, thus opening the way to utilize light incident on the entire image sensor area. Compared to the conventional image sensors whose subpixels only utilize either a quarter (red and blue) or half (green) of the incident light, the color splitters can, in principle, exhibit 2 to 4 times higher optical efficiencies.

Metasurface-based color splitter is configured by allocating dielectrics of different refractive indices inside the design region. This is a typical freeform optimization problem involving high degrees of freedom (DoF). There have been many attempts to solve such optimization problems. The first measurement data in the visible range was reported by Miyata et al.⁴ The authors used a conventional library-based meta-atom method to design a single-layer color splitter. Although a library-based method has a significantly constrained design space, the fabricated device already showed superior performance compared to the classical color filter. Similar work was followed by Zou et al. who designed a single-layer freeform color splitter using the genetic algorithm and measured its performance in the visible range.⁵ Investigation on multilayer devices has also been reported. Although a multilayer device tends to show higher performance, the design optimization of a multilayer device is much harder than that of a single-layer device due to the large DoF. A typical approach to handle this large DoF is to utilize local figure-of-merit gradients on design variables obtained through auto-gradient calculation⁶ or the adjoint method.^{7,8} Zhao et al.⁹ and Catrysse et al.¹⁰ optimized high-complexity color splitters in 2D and 3D space using auto-gradient calculations. The design space is meshed with ultra-fine grids, and the authors were able to obtain a device design with near-perfect efficiency. Another pioneering work was done by Camayd-Muñoz et al. where an adjoint-based method was applied to design a 3D device with a higher fabricability. Despite the rapidly growing field,^{11–20} there has not been any systematic investigation into the choice of device design parameters. The choice of design parameters, such as the device height or selection of refractive index, has a critical effect on the final optimized devices. Until now, the choice of such parameters was based on simple deductions such as Fabry-Perot resonance conditions or even worse, based on the computational resource availability.¹⁶

In this work, we outline the effect of design parameters on the optimized optical efficiency of a color splitter. The result shows that there exist optimal ranges of both structural parameters and the optical index contrast of constituting materials, and more interestingly, their optimal ranges are correlated with each other. We also investigate how the spatial grid size and the number of grid layers affect the optical efficiency and demonstrate that a sufficiently high-performing device can be obtained even with a large cell size if a sufficient number of layers are deposited. This highlights the important role that the choice of design parameters plays in determining the device's performance.

¹School of Electrical Engineering, Korea Advanced Institute of Science and Technology, Daejeon 34141, Republic of Korea

²Department of Electronic Engineering, Hanyang University, Seoul 04763, South Korea

³Department of Artificial Intelligence, Hanyang University, Seoul 04763, South Korea

⁴These authors contributed equally

⁵Lead contact

*Correspondence: jang.minseok@kaist.ac.kr

<https://doi.org/10.1016/j.isci.2023.107788>



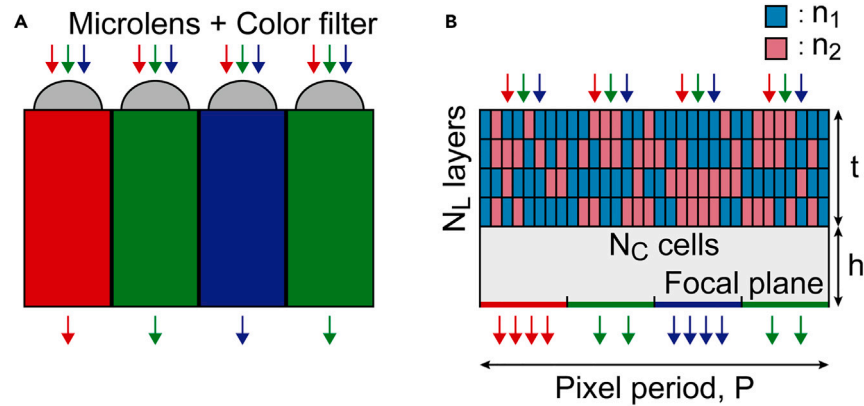


Figure 1. Schematic of the working principle

(A) A simplified diagram of a conventional image sensor consisting of a microlens array and color filter.

(B) A schematic diagram of a color splitter. The design area ($P \times t$) is gridded into a grid of $N_C \times N_L$, and refractive indices n_1 and n_2 are allocated to each cell for color splitting. Two and four arrows at the focal plane of the color splitter imply that an ideal color splitter can have a two-fold, four-fold increase in optical efficiency compared to the conventional design.

RESULTS

As schematically shown in Figures 1B and 1A, the color splitter deflects the incident light to its corresponding subpixel area. Instead of forming a lens-like structure, the design area is gridded into rectangular cells, and each cell is filled with a selection of two different dielectrics. The design parameters for the 2D color splitters can be classified into two categories: physical parameters and spatial resolution parameters. The physical parameters include color splitter period (P), thickness (t), the position of the focal plane (h), and the refractive indices of the two composing dielectrics (n_1 and n_2). The spatial resolution, determined by the number of grid layer N_L and the grid elements in a layer N_C , defines how the design area is gridded into cells of equal shape. Consequently, the design problem possesses $N_L \times N_C$ DoF and thus the number of possible structures is $2^{N_L N_C}$. The default values of each design parameter are given in Table 1. As the transition from geometric optics to wave optics occurs for geometries with characteristic lengths comparable to or smaller than the wavelength, the color splitter configured with the default design parameters lies within the wave optics regime.

In this work, we define the optical efficiency $\eta(\lambda)$ using the electric field intensity at the focal plane (denoted by the dashed line in Figures 2A–2C).

$$\eta_{R,G,B}(\lambda) = \frac{1}{2} \sum_{i=TE,TM} \frac{\int_{x_1}^{x_2} |E(\lambda, i)|^2 dx}{\int_0^P |E(\lambda, i)|^2 dx} \times T(\lambda, i)$$

Here, E is the electric field at the focal plane, and T is the transmittance. Electric field distribution and the total transmittance are calculated with RETICOLO, a rigorous coupled-wave analysis package.²¹ $x \in (x_1, x_2)$ defines the area of the subpixel of interest. For simplicity, we assume that the wavelength range required for red (R), green (G), and blue (B) subpixels are 600 nm–700 nm, 500–600 nm, and 400 nm–500 nm, respectively. Throughout the work, a normally incident light is assumed, and the optical efficiency is averaged between both transverse electric (TE) and transverse magnetic (TM) polarizations. Figures 2A–2C show the electric field intensity distribution inside an optimized color splitter with the default design parameters listed in Table 1. Figure 2D shows the electric field intensity distribution on the surface of the photodetectors. The optical efficiency $\eta_{R,G,B}(\lambda)$ of the same device is shown as red, green, and blue curves in Figure 2E. The peak optical efficiencies within red (600–700 nm), green (500–600 nm), and blue (400–500 nm) regions are 70.12% (669 nm), 57.15% (554 nm), and 77.39% (422 nm), respectively, which are comparable to those reported in other related works (see Table S1 for comparison).^{5,7,9,10,16,18} Both the field distributions and the optical efficiency plots clearly show that the intensity of light is concentrated at the corresponding subpixel area on the focal plane. The optimized device possesses an optical crosstalk of 16.8% (see Figure S1 for detailed analysis). The optical efficiency drops rapidly as the angle of incidence (θ) deviates from normal to the surface. The color splitting effect still remains for $\theta \leq 7^\circ$ but the efficiency becomes as low as 45.6% at $\theta = 5^\circ$ as discussed in Figure S2.

In a conventional Bayer-type image sensor, a pixel consists of two green subpixels and one subpixel for red and blue, respectively. In order to account for such a subpixel ratio, we include two green subpixels in one period of a 1D image sensor. The default arrangement of the subpixels in this paper was set to RGBG as the design is periodic and the wavelength of the green light is in between red and blue (Figure 1B). In Figure S3, we compare the optical efficiency between the RGBG subpixel arrangement and the RGGB subpixel

Table 1. The default design parameters used in this work

Design parameter	Value
Pixel period, P	1 μm (equivalent to subpixel size of 0.25 μm)
Thickness of the color splitter, t	1.5 μm
Refractive index of dielectric 1, n_1	1.5
Refractive index of dielectric 2, n_2	2.0
Position of the focal plane, h	0.5 μm
Number of grid layers (N_L)	4
Number of cells in a layer (N_C)	32

arrangement. As Figure S3 suggests, the arrangement of subpixels has a marginal effect on the device performance in terms of optical efficiency and crosstalk.

To understand how the design parameters of a color splitter affect its performance, we optimize the device geometry for various choices of design parameters. For given device design parameters, a conventional genetic algorithm with elitism is performed to obtain the optimal dielectric distribution in the grids.^{22,23} The optimization is configured with a population size of 200, and 100 epochs. The genotype of the individuals in the gene pool is represented by a binary array with array dimensions equal to N_C and N_L . The goal of the optimization is to maximize the average optical efficiency, $\bar{\eta} = (\bar{\eta}_R + \bar{\eta}_G + \bar{\eta}_B)/3$, where $\bar{\eta}_{R,G,B}$ are the wavelength-averaged optical efficiencies obtained by averaging $\eta_{R,G,B}(\lambda)$ over the wavelength range corresponding to the subpixel type. During the optimization process, the optical efficiencies

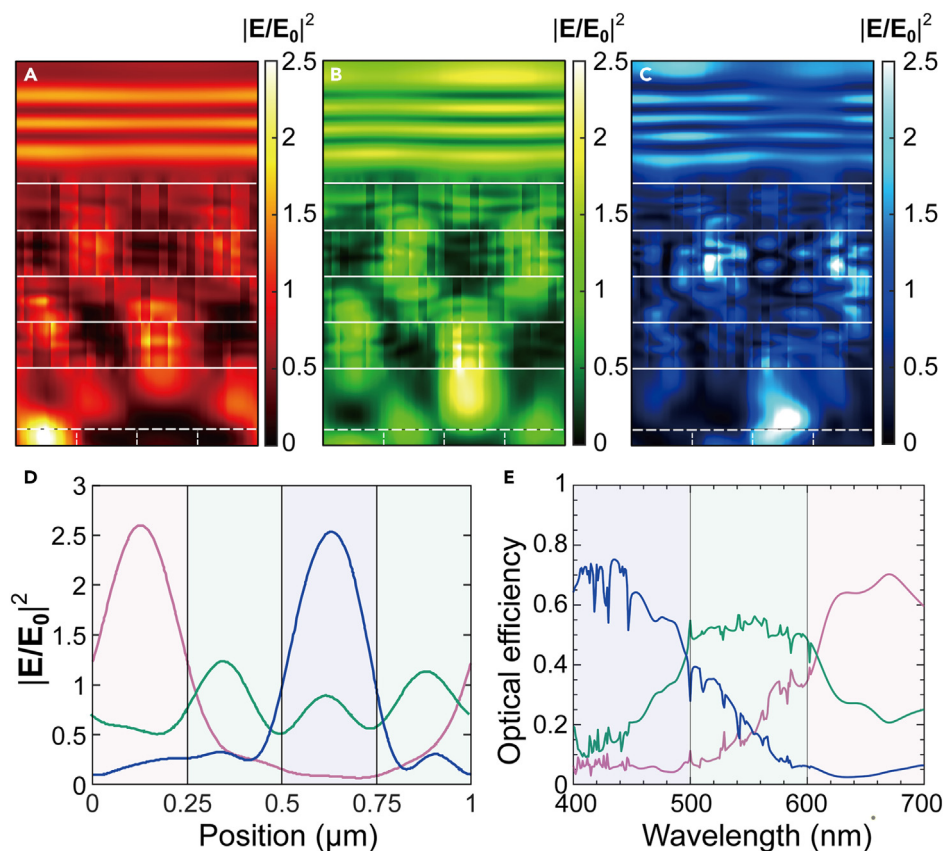


Figure 2. Performance of the optimized device

(A–C) The electric field intensity profile inside the optimized device is given in Figure 1B for a normally incident light of (a) $\lambda = 650$ nm, (b) $\lambda = 550$ nm, (c) $\lambda = 450$ nm.

The depicted field distribution is the average of transverse electric and transverse magnetic polarized light.

(D) The electric field intensity profile of red, green, and blue normally incident light on the surface of the photodetector.

(E) Optical efficiency spectra of the same device. The default design parameters in Table 1 are used. The average optical efficiency is 58.29%. The device sorts red, green, and blue normal incident light with peak efficiencies of up to 70.12%, 57.15%, and 77.39% at 669 nm, 554 nm, and 422 nm wavelengths, respectively.

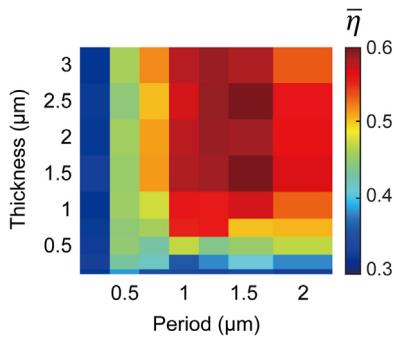


Figure 3. Dependency of design parameters: Period and thickness

Effect of device period (P) and color splitter thickness (t) on the optical efficiency of a color splitter. N_L and N_C are fixed to (4, 32). The design parameters stated in Table 1 are used except for P , and t .

were averaged over thirty wavelength points (405 nm, 415 nm, ... 695 nm) to reduce the computational cost, but the reported $\bar{\eta}$ were averaged over with much finer wavelength points (400 nm, 401 nm, ... 700 nm). As shown in Figure S4, the difference between 30 and 301 wavelength-point averaging is not significant (around 0.02 for $(N_L, N_C) = (8, 64)$ and 0.01 for $(N_L, N_C) = (4, 32)$).

The advantage of substituting microlens and color filters with metasurface-based color splitters becomes clear for sub-micron image sensors. Hence, we first investigate the effect of the physical dimensions of devices on the optical efficiency of the splitter. It should be noted that the subpixel size of the 2D color splitter is a quarter of the device period, P . In comparison to a Bayer-type image sensor array, a 2D color splitter extends infinitely in the y -direction so the pixel size is defined as the width of each subpixel in the x -direction. The pixel size of the color splitter with the default design parameter is $0.25 \mu\text{m}$, which is less than half the size of the smallest commercially available image sensor of $\sim 0.56 \mu\text{m}$.³ Figure 3 shows how the optimized $\bar{\eta}$ varies depending on the period P and the thickness t while all the other design parameters including DoF and refractive indices are fixed to their default values. For the devices with a deep subwavelength period of $p = 0.25 \mu\text{m}$, the optimized average optical efficiencies are around the trivial value of 33%, which can be achieved with a simple antireflection layer. When $p \geq 0.5 \mu\text{m}$, the color splitters start to show meaningful performance. At a given P , the device performance monotonically increases and saturates as the thickness t increases. The saturation point of t for $0.75 \mu\text{m} \leq p \leq 2 \mu\text{m}$ is around $1.5 \mu\text{m}$, and thus we set $t = 1.5 \mu\text{m}$ as the default value. We note that, however, the saturation point of t can vary as a function of the other design parameters. At a fixed t , the optimized $\bar{\eta}$ does not monotonically increase with P but has a specific optimal value. This result is reasonable since it becomes increasingly difficult to split incident light over a longer lateral distance within a given thickness.

The position of the focal plane from the color splitter, h , is a similar physical design parameter to P and t , which also defines the physical dimension of the device. The dependence of the focal plane position on the optical efficiency is shown in Figure S5. In a periodic grating, the modes with a high lateral wavenumber cannot be extracted in the far field. Hence, as the focal plane of the color splitter is located further from the meshed region, the device is expected to have a lower efficiency due to the loss of near field. The sharp drop in optical efficiency for $h > 1 \mu\text{m}$ in Figure S5 agrees with this expectation.

The refractive indices of the composing dielectric materials are another critical factor determining optimal efficiency. In previous works, the selection of a color splitter was based on simple relations such as the Fabry-Perot resonance condition.¹⁶ Those relations only provide order-of-magnitude estimates. In this work, we tune the design parameters (t, n_1, n_2) to find the global trend in optimized optical efficiency. For the sake of simplicity, we assume that the dielectrics filling each grid are dispersionless and have refractive indices of n_1 and n_2 , where $n_1 \leq n_2$ is assumed throughout the work. The default values of (n_1, n_2) are (1.5, 2.0), which is similar to the refractive indices of silica and silicon nitride. Our analyses reveal that, unlike other nanophotonic devices such as metalens whose device performance monotonically increases with the refractive index contrast,^{24–26} color splitters have a distinct relation between

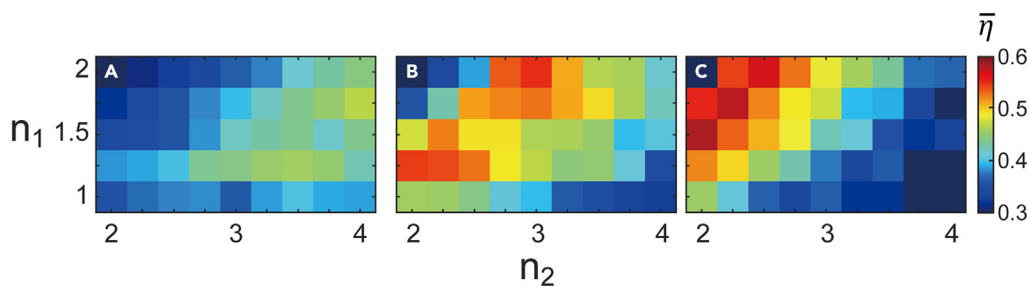


Figure 4. Dependency of design parameters: Refractive indices and thickness

Effect of refractive indices on the optical efficiency for different device thicknesses, t .

(A–C) Optimization based on a genetic algorithm was carried out for color splitters with thickness (a) $t = 0.1 \mu\text{m}$, (b) $t = 0.5 \mu\text{m}$, and (c) $t = 1.5 \mu\text{m}$. In each color plot, the lower refractive index n_1 is changed from 1 to 2 with a step size of 0.25, and n_2 is swept from 2 to 4 with the same step size, 0.25. Each square represents the optimized efficiency obtained with the genetic algorithm. The maximum efficiency in each case is (a) 46.86%, (b) 54.98%, (c) 58.25%. Except for t, n_1 , and n_2 , the design parameters given in Table 1 are used.

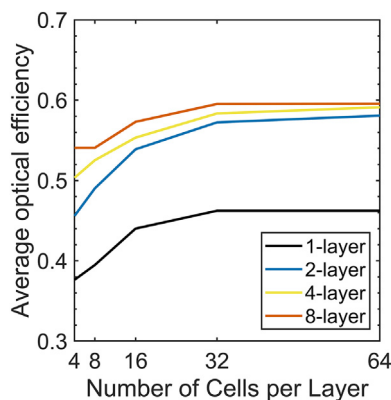


Figure 5. Dependency of design parameters: Degree of freedom

Optimized optical efficiency calculated for multiple DoF configurations.

The optical efficiency saturates to $\sim 60\%$. Except for N_L and N_C , the design parameters given in Table 1 are used.

the optimal refractive index contrast and the thickness of the device. When all the other parameters are fixed to their default values, the optimal index contrast values, $n_1 - n_2$, are found to be 2.25, 1, and 0.5 for $t = 0.1, 0.5$, and $1.5 \mu\text{m}$, respectively, as illustrated in Figure 4. We speculate that the trend could be attributed to the fact that the maximum achievable vertical optical path length difference is determined by the product of optical index contrast and the thickness of the device.

The choice of DoF is important in both computational and experimental aspects. On the computational side, the design space grows exponentially with the DoF, and the computational load required for optimization grows accordingly. Popular approaches for tackling high DoF problems are through the adjoint gradient, which provides the gradient of FoM with respect to change in the refractive index of every element in the design space,^{23,27–34} or through machine learning methods.^{35–43} In our work, we limit the DoF to the order of hundreds so that the optimization problem is solvable using the classical genetic algorithm.^{22,44–47} On the other hand, the DoF is directly related to the fabrication feasibility of the device. The number of layers, N_L , determines the number of deposition steps, and the number of cells in a layer, N_C , affects the minimum feature size. Despite its importance, previous works on metasurface-based color splitters mostly lack investigations on DoF. In this work, we fix the values of the other design parameters including the device thickness, and change N_L and N_C to isolate the effect arising from the device dimension change. N_L and N_C are chosen to be integer powers of 2. This implies the existence of trivial monotonicity. For example, a set of every possible combination with ($N_L = 1, N_C = 8$) is a subset of ($N_L = 4, N_C = 16$) so the optical efficiency of the latter must be equal to or greater than the previous one if the optimization converges to the global optimum. Since the number of possible combinations is sufficiently low for device designs with $\text{DoF} \leq 16$, an exhaustive search was carried out for the corresponding conditions. For device designs with $\text{DoF} \geq 32$, the previously-described genetic algorithm was carried out.

Figure 5 shows the optimized results for each N_L and N_C pair. In the figure, the trivial monotonic relation in the optimized efficiency is observed. Regardless of the number of layers, the optimal $\bar{\eta}$ almost saturates when $N_C \geq 32$, which corresponds to the minimum feature size of $\sim 31 \text{ nm}$. The optimal $\bar{\eta}$ asymptotically approaches $\sim 60\%$ for the default physical parameters. It is important to note that, the number of layers N_L plays a pivotal role in determining the device performance. For example, even with $N_C = 4$ (minimum feature size of 250 nm), it is possible to achieve the average optical efficiency of $\sim 54\%$ (about 90% of the highest efficiency achieved in this work) by having 8 layers. A similar trend was found when N_L is increased while keeping the thickness of each layer to be 375 nm as shown in Figure S6. The designs of color splitters for different DoF conditions are displayed in Figure S7. For low-efficiency devices, a line of reflection symmetry exists at the center of the red and blue subpixel. This line of reflection symmetry originates from RGBG subpixel arrangement which is also symmetric with respect to that line. However, such reflection symmetry isn't observed in the optimized devices. The lack of symmetry in the optimized devices implies that the enforcement of trivial symmetry conditions on the device design does not always lead to better performance. Finally, we note that the optical efficiency of a color splitting device can surpass what has been reported in this work and even reach near unity when the device is optimized with significantly higher DoF.⁹

DISCUSSION

In conclusion, we systematically analyze the dependence of color splitter performance on various design parameters by leveraging numerical device optimization methods based on a genetic algorithm. We discover that the average optical efficiency of a color splitter with a micron-scale form factor can be up to $\sim 60\%$, whereas the classical microlens and color filter configuration can have optical efficiency of up to 25% for red and blue and 50% for green. We show that it is not always beneficial to have a larger pixel if the thickness of the device is limited and there exist optimal refractive index pairs for composing dielectrics for a given device thickness. Unlike the case of metalens, the optical efficiency drops when the refractive index contrast becomes greater than the optimal value. We also report that the device performance can be greatly increased while maintaining a relatively large feature size by having multiple layers in the design scheme. We anticipate that the qualitative trend seen in the 2D color splitter design parameter tuning would be repeated for Bayer-type 3D color splitters, although the optimal values may differ due to the introduction of the additional dimension. Our results will serve as a design guideline for the future development of free-form metasurface-based color splitters for deep sub-micron image sensors.

Limitations of the study

In this research, we computed the optical efficiency based on the electric field distribution at the focal plane. However, for the practical utilization of the device as a color router in image sensors, a more appropriate measure of optical efficiency would involve considering the absorption at the photodiode region beneath the color router. Incorporating such structures into the simulation domain introduces complexities, as the electric field distribution is influenced by reflections from these intricate elements. In our study, we simplified the situation by excluding the photodiode and electric circuits beneath the color router, substituting them with infinitely deep dielectrics. This approach allowed us to focus on the impact of the device design parameters on color sorting efficiency while sidestepping the added intricacies stemming from the inclusion of these additional elements.

STAR★METHODS

Detailed methods are provided in the online version of this paper and include the following:

- KEY RESOURCES TABLE
- RESOURCE AVAILABILITY
 - Lead contact
 - Materials availability
 - Data and code availability
- EXPERIMENTAL MODEL AND SUBJECT DETAILS
- METHOD DETAILS
- QUANTIFICATION AND STATISTICAL ANALYSIS
- ADDITIONAL RESOURCES

SUPPLEMENTAL INFORMATION

Supplemental information can be found online at <https://doi.org/10.1016/j.isci.2023.107788>.

ACKNOWLEDGMENTS

This research was supported by the MOTIE (Ministry of Trade, Industry & Energy 1415180303 and KSRC (Korea Semiconductor Research Consortium) 20019357 support program for the development of the future semiconductor device.

AUTHOR CONTRIBUTIONS

Sanmun K. and M.S.J. conceived the ideas. Sanmun K., C.P., and Shinho K. developed the optical simulation model and the optimization algorithms. Sanmun K., C.P., and M.S.J. conducted a detailed analysis of the optimization results. M.S.J. supervised the project. The manuscript was mainly written by Sanmun K., C.P., and M.S.J. with the contributions of all authors.

DECLARATION OF INTERESTS

The authors declare no conflicts of interest.

Received: March 28, 2023

Revised: August 28, 2023

Accepted: August 29, 2023

Published: September 15, 2023

REFERENCES

1. Chung, H., Zhou, Z., and Bermel, P. (2017). Collimated thermal radiation transfer via half Maxwell's fish-eye lens for thermophotovoltaics. *Appl. Phys. Lett.* *110*, 201111. <https://doi.org/10.1063/1.4983679>.
2. Catrysse, P.B., and Wandell, B.A. (2002). Optical efficiency of image sensor pixels. *J. Opt. Soc. Am. A* *19*, 1610–1620. <https://doi.org/10.1364/JOSAA.19.001610>.
3. Samsung-Newsroom (2022). Samsung Unveils ISOCELL Image Sensor with Industry's Smallest 0.56µm Pixel.
4. Miyata, M., Nemoto, N., Shikama, K., Kobayashi, F., and Hashimoto, T. (2021). Full-color-sorting metalenses for high-sensitivity image sensors. *Optica* *8*, 1596–1604. <https://doi.org/10.1364/OPTICA.444255>.
5. Zou, X., Zhang, Y., Lin, R., Gong, G., Wang, S., Zhu, S., and Wang, Z. (2022). Pixel-level Bayer-type colour router based on metasurfaces. *Nat. Commun.* *13*, 3288. <https://doi.org/10.1038/s41467-022-31019-7>.
6. Paszke, A., Gross, S., Chintala, S., Chanan, G., Yang, E., DeVito, Z., Lin, Z., Desmaison, A., Antiga, L., and Lerer, A. (2017). Automatic Differentiation in Pytorch.
7. Camayd-Muñoz, P., Ballew, C., Roberts, G., and Faraon, A. (2020). Multifunctional volumetric meta-optics for color and polarization image sensors. *Optica* *7*, 280–283. <https://doi.org/10.1364/OPTICA.384228>.
8. Campbell, S.D., Sell, D., Jenkins, R.P., Whiting, E.B., Fan, J.A., and Werner, D.H. (2019). Review of numerical optimization techniques for meta-device design [Invited]. *Opt. Mater. Express* *9*, 1842–1863. <https://doi.org/10.1364/Ome.9.001842>.
9. Zhao, N., Catrysse, P.B., and Fan, S. (2021). Perfect RGB-IR Color Routers for Sub-Wavelength Size CMOS Image Sensor Pixels. *Advanced Photonics Research* *2*, 2000048. <https://doi.org/10.1002/adpr.202000048>.
10. Catrysse, P.B., Zhao, N., Jin, W., and Fan, S. (2022). Subwavelength Bayer RGB color routers with perfect optical efficiency.

- Nanophotonics 11, 2381–2387. <https://doi.org/10.1515/nanoph-2022-0069>.
11. Chen, M., Wen, L., Pan, D., Cumming, D.R.S., Yang, X., and Chen, Q. (2021). Full-color nanorouter for high-resolution imaging. *Nanoscale* 13, 13024–13029. <https://doi.org/10.1039/D1NR02166D>.
 12. Li, J., Cao, M., Liang, W., Zhang, Y., Xie, Z., and Yuan, X. (2022). Inverse design of 1D color splitter for high-efficiency color imaging. *Chin. Opt. Lett.* 20, 073601.
 13. Miyata, M., Nakajima, M., and Hashimoto, T. (2019). High-Sensitivity Color Imaging Using Pixel-Scale Color Splitters Based on Dielectric Metasurfaces. *ACS Photonics* 6, 1442–1450. <https://doi.org/10.1021/acsp Photonics.9b00042>.
 14. Chen, Q., Nan, X., Chen, M., Pan, D., Yang, X., and Wen, L. (2021). Nanophotonic Color Routing. *Adv. Mater.* 33, 2103815. <https://doi.org/10.1002/adma.202103815>.
 15. Roberts, G., Ballew, C., Zheng, T., Garcia, J.C., Camayd-Muñoz, S., Hon, P.W., and Faraon, A. (2022). 3D-Patterned Inverse-Designed Mid-Infrared Metaoptics preprint at arXiv. <https://doi.org/10.48550/arXiv.2209.07553>.
 16. Li, J., Chen, Q., Li, G., Li, Y., Zhang, Y., Li, C., Bai, L., Zhong, R., He, Y., Xu, F., et al. (2022). Single-Layer Bayer Metasurface via Inverse Design. *ACS Photonics* 12, 2607–2615. <https://doi.org/10.1021/acsp Photonics.2c00990>.
 17. Park, J., Jeon, S., and Kim, S.J. (2021). Subwavelength, polarimetric color sorting by densely interleaved nano-resonators. *Opt Commun.* 485, 126711. <https://doi.org/10.1016/j.optcom.2020.126711>.
 18. Zou, X., Gong, G., Lin, Y., Fu, B., Wang, S., Zhu, S., and Wang, Z. (2023). Metasurface-based polarization color routers. *Opt Laser Eng.* 163, 107472. <https://doi.org/10.1016/j.optlaseng.2022.107472>.
 19. Jin, Z., Mei, S., Chen, S., Li, Y., Zhang, C., He, Y., Yu, X., Yu, C., Yang, J.K.W., Luk'yanchuk, B., et al. (2019). Complex Inverse Design of Meta-optics by Segmented Hierarchical Evolutionary Algorithm. *ACS Nano* 13, 821–829. <https://doi.org/10.1021/acsnano.8b08333>.
 20. Johlin, E. (2021). Nanophotonic color splitters for high-efficiency imaging. *iScience* 24, 102268. <https://doi.org/10.1016/j.isci.2021.102268>.
 21. Hugonin, J.P., and Lalanne, P. (2021). Reticolo software for grating analysis preprint at arXiv. <https://doi.org/10.48550/arXiv.2101.00901>.
 22. Park, J., Kim, S., Lee, J., Menabde, S.G., and Jang, M.S. (2019). Ultimate Light Trapping in a Free-Form Plasmonic Waveguide. *Phys. Rev. Appl.* 12, 024030. <https://doi.org/10.1103/PhysRevApplied.12.024030>.
 23. Park, J., Kim, S., Nam, D.W., Chung, H., Park, C.Y., and Jang, M.S. (2022). Free-form optimization of nanophotonic devices: from classical methods to deep learning. *Nanophotonics* 11, 1809–1845. <https://doi.org/10.1515/nanoph-2021-0713>.
 24. Bayati, E., Zhan, A., Colburn, S., Zhelyeznyakov, M.V., and Majumdar, A. (2019). Role of refractive index in metalens performance. *Appl. Opt.* 58, 1460–1466. <https://doi.org/10.1364/AO.58.001460>.
 25. Martin, O.J.F., and Piller, N.B. (1998). Electromagnetic scattering in polarizable backgrounds. *Phys. Rev. E* 58, 3909–3915. <https://doi.org/10.1103/PhysRevE.58.3909>.
 26. Sihvola, A., and Lindell, I.V. (1989). Polarizability and Effective Permittivity of Layered and Continuously Inhomogeneous Dielectric Spheres. *J. Electromagn. Waves Appl.* 3, 37–60. <https://doi.org/10.1163/15693989X000043>.
 27. Sell, D., Yang, J., Doshay, S., Yang, R., and Fan, J.A. (2017). Large-Angle, Multifunctional Metagratings Based on Freeform Multimode Geometries. *Nano Lett.* 17, 3752–3757. <https://doi.org/10.1021/acsnanolett.7b01082>.
 28. Christiansen, R.E., Lin, Z., Roques-Carnes, C., Salamin, Y., Kooi, S.E., Joannopoulos, J.D., Soljačić, M., and Johnson, S.G. (2020). Fullwave Maxwell inverse design of axisymmetric, tunable, and multi-scale multi-wavelength metalenses. *Opt Express* 28, 33854–33868. <https://doi.org/10.1364/OE.403192>.
 29. Sitawarin, C., Jin, W., Lin, Z., and Rodriguez, A.W. (2018). Inverse-designed photonic fibers and metasurfaces for nonlinear frequency conversion [Invited]. *Photon. Res.* 6, B82–B89. <https://doi.org/10.1364/PRJ.6.000882>.
 30. Sapra, N.V., Yang, K.Y., Vercrussey, D., Leadle, K.J., Black, D.S., England, R.J., Su, L., Trivedi, R., Miao, Y., Solgaard, O., et al. (2020). On-chip integrated laser-driven particle accelerator. *Science* 367, 79–83. <https://doi.org/10.1126/science.aay5734>.
 31. Wang, F., Qiao, G., and Lou, X. (2011). Robust topology optimization of photonic crystal waveguides with tailored dispersion properties. *J. Neuro Oncol.* 104, 387–394. <https://doi.org/10.1364/JOSAB.28.000387>.
 32. Jensen, J.S., and Sigmund, O. (2004). Systematic design of photonic crystal structures using topology optimization: Low-loss waveguide bends. *Appl. Phys. Lett.* 84, 2022–2024. <https://doi.org/10.1063/1.1688450>.
 33. Chung, H., and Miller, O.D. (2020). High-NA achromatic metalenses by inverse design. *Opt Express* 28, 6945–6965. <https://doi.org/10.1364/OE.385440>.
 34. Chung, H., Park, J., and Boriskina, S.V. (2022). Inverse-designed waveguide-based biosensor for high-sensitivity, single-frequency detection of biomolecules. *Nanophotonics* 11, 1427–1442. <https://doi.org/10.1515/nanoph-2022-0012>.
 35. Kim, S., Shin, J.M., Lee, J., Park, C., Lee, S., Park, J., Seo, D., Park, S., Park, C.Y., and Jang, M.S. (2021). Inverse design of organic light-emitting diode structure based on deep neural networks. *Nanophotonics* 10, 4533–4541. <https://doi.org/10.1515/nanoph-2021-0434>.
 36. Seo, D., Nam, D.W., Park, J., Park, C.Y., and Jang, M.S. (2022). Structural Optimization of a One-Dimensional Freeform Metagrating Deflector via Deep Reinforcement Learning. *ACS Photonics* 9, 452–458. <https://doi.org/10.1021/acsp Photonics.1c00839>.
 37. Ma, W., Cheng, F., Xu, Y., Wen, Q., and Liu, Y. (2019). Probabilistic Representation and Inverse Design of Metamaterials Based on a Deep Generative Model with Semi-Supervised Learning Strategy. *Adv. Mater.* 31, 1901111. <https://doi.org/10.1002/adma.201901111>.
 38. Jiang, J., Sell, D., Hoyer, S., Hickey, J., Yang, J., and Fan, J.A. (2019). Free-Form Diffractive Metagrating Design Based on Generative Adversarial Networks. *ACS Nano* 13, 8872–8878. <https://doi.org/10.1021/acsnano.9b02371>.
 39. Fang, Z., and Zhan, J. (2020). Deep Physical Informed Neural Networks for Metamaterial Design. *IEEE Access* 8, 24506–24513. <https://doi.org/10.1109/ACCESS.2019.2963375>.
 40. An, S., Zheng, B., Tang, H., Shalaginov, M.Y., Zhou, L., Li, H., Kang, M., Richardson, K.A., Gu, T., Hu, J., et al. (2021). Multifunctional Metasurface Design with a Generative Adversarial Network. *Adv. Opt. Mater.* 9, 2001433. <https://doi.org/10.1002/adom.202001433>.
 41. So, S., and Rho, J. (2019). Designing nanophotonic structures using conditional deep convolutional generative adversarial networks. *Nanophotonics* 8, 1255–1261. <https://doi.org/10.1515/nanoph-2019-0117>.
 42. So, S., Badloe, T., Noh, J., Bravo-Abad, J., and Rho, J. (2020). Deep learning enabled inverse design in nanophotonics. *Nanophotonics* 9, 1041–1057. <https://doi.org/10.1515/nanoph-2019-0474>.
 43. Jiang, J., and Fan, J.A. (2019). Global Optimization of Dielectric Metasurfaces Using a Physics-Driven Neural Network. *Nano Lett.* 19, 5366–5372. <https://doi.org/10.1021/acsnanolett.9b01857>.
 44. Huang, Y., Zhen, Z., Shen, Y., Min, C., and Veronis, G. (2019). Optimization of photonic nanojets generated by multilayer microcylinders with a genetic algorithm. *Opt Express* 27, 1310–1325. <https://doi.org/10.1364/OE.27.001310>.
 45. Jafar-Zanjani, S., Inampudi, S., and Mosallaei, H. (2018). Adaptive Genetic Algorithm for Optical Metasurfaces Design. *Sci. Rep.* 8, 11040. <https://doi.org/10.1038/s41598-018-29275-z>.
 46. Lee, W.-K., Yu, S., Engel, C.J., Reese, T., Rhee, D., Chen, W., and Odom, T.W. (2017). Concurrent design of quasi-random photonic nanostructures. *Proc. Natl. Acad. Sci. USA* 114, 8734–8739. <https://doi.org/10.1073/pnas.1704711114>.
 47. Yu, Z., Cui, H., and Sun, X. (2017). Genetic-algorithm-optimized wideband on-chip polarization rotator with an ultrasmall footprint. *Opt. Lett.* 42, 3093–3096. <https://doi.org/10.1364/OL.42.003093>.

STAR★METHODS

KEY RESOURCES TABLE

REAGENT or RESOURCE	SOURCE	IDENTIFIER
Software and algorithms		
MATLAB	MathWorks Co., LTD.	https://www.mathworks.com/products/matlab.html

RESOURCE AVAILABILITY

Lead contact

Further information and requests for resources and reagents should be directed to and will be fulfilled by the lead contact, Min Seok Jang (jang.minseok@kaist.ac.kr).

Materials availability

This study did not generate new unique reagents.

Data and code availability

- Data reported in this paper will be shared by the [lead contact](#) upon request.
- The optimization code can be accessed openly on GitHub (<https://github.com/chocopi2718/colorRouter2D>).
- Any additional information required to reanalyze the data reported in this paper is available from the [lead contact](#) upon request

EXPERIMENTAL MODEL AND SUBJECT DETAILS

The MATLAB software has been employed to optimize the optical efficiency of the color splitter.

METHOD DETAILS

The simulation is conducted with the MATLAB software.

QUANTITATION AND STATISTICAL ANALYSIS

The simulation data is produced by MATLAB software. Figures shown in the main text were produced by MATLAB and Adobe illustrator from the raw data.

ADDITIONAL RESOURCES

Any additional information about the simulation and data reported in this paper is available from the [lead contact](#) on request.